Characterizing the Temperature Sensitivity of the Hartmann Sensor

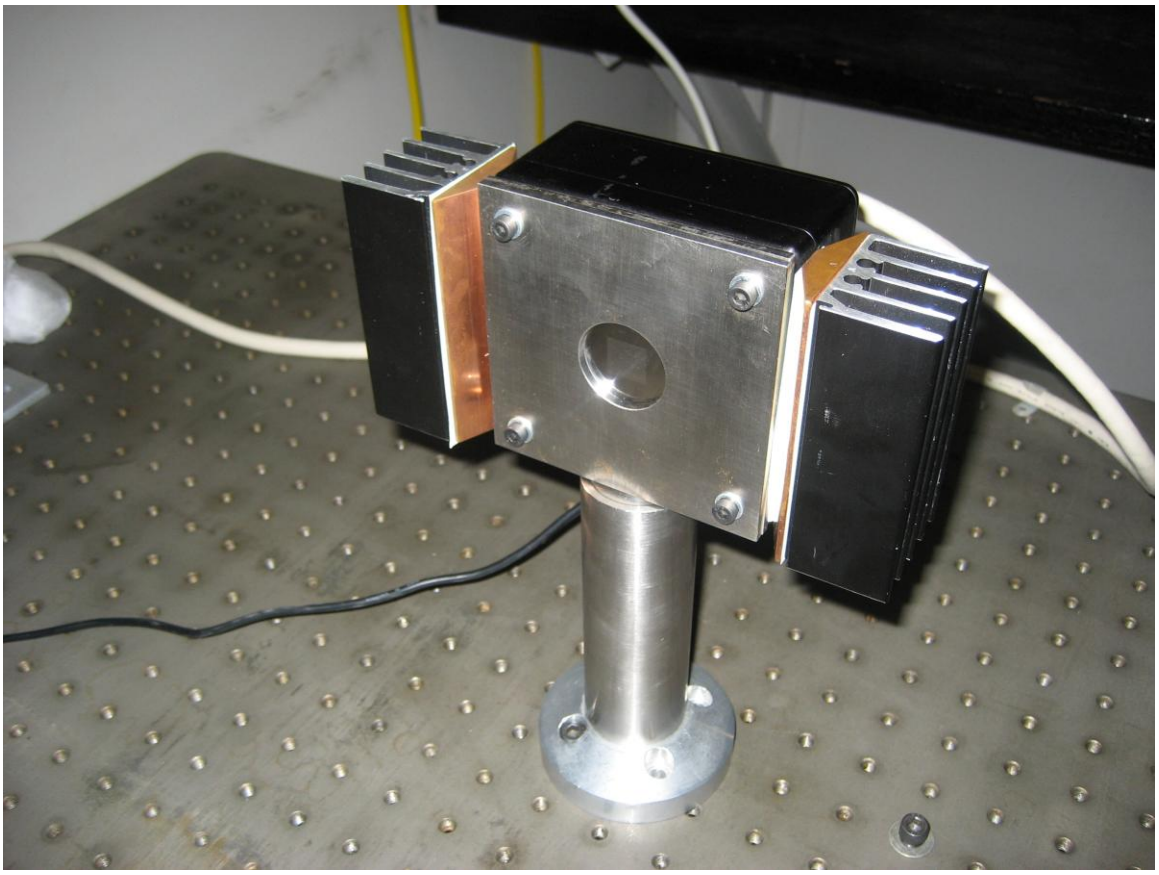

Picture of the Hartmann Sensor in the Optics Lab, University of Adelaide

Kathryn Meehan
June 2 –July 30, 2010
Optics and Photonics Group
University of Adelaide

ABSTRACT

This paper discusses our search for the source of the cylindrical component of the wavefront aberration signal measured and our search for possible causes for the rms values to be significantly poorer than expected when the frames are not shuffled. Although no definite cause has been identified, we have conducted testing on a more in-depth level than had been done previously and have come closer to understanding which mechanisms may or may not be at fault. We found that factors such as heating method, method of subtracting prism, replacing the camera, using heat sinks, or using the brass and aluminum set-up in place of the invar set-up did not affect our results. However, we discovered that slight air disturbances had a great effect on the centroid displacement.

Introduction

A Motive

An international collaboration of scientists is working to make Advanced LIGO (Laser Interferometer Gravitational Wave Observatory) more sensitive than initial LIGO by over a factor of 10. It is predicted that the Advanced LIGO will be able to detect a gravitational wave roughly once a week, a vast improvement from the initial LIGO which is expected to make a detection approximately once every 50 years. The power in the Fabry-Perot cavities of the Advanced LIGO is expected to be on the order of 1 MW[1]. These improvements require simultaneous technological developments in the correction system used to maintain proper functioning of the detector. To maximize the sensitivity of Advanced LIGO and effectively compensate for wavefront distortions such as those due to thermal lensing, it is important to have a wavefront sensor that is able to accurately measure those distortions. The Optics and Photonics group at the University of Adelaide has developed a Hartmann wavefront sensor with a precision of $\lambda/15{,}500$ and an accuracy of $\lambda/3{,}300$ at a measurement wavelength of 800 nm[2]. Due to its ultra-sensitivity, it has been selected to be used in Advanced LIGO.

The Hartmann sensor is a type of wavefront sensor that can both detect wavefronts and changes in wavefronts. The Shack-Hartmann sensor is one type of Hartmann sensor that is used frequently, especially by astronomers. It uses a micro-lens array and is very light efficient, but cannot make measurements with high precision. The sensor that the University of Adelaide is developing is a Hartmann wavefront sensor which is not as light efficient but can make highly accurate measurements and is thus more suited for gravitational wave detection.

B. Hartmann Wavefront Sensor Basics

The light source being used is a single mode fiber coupled laser diode that emits at $\lambda = 980$ nm. The Hartmann plate, shown in Figure 1, consists of an array of 1,024 holes. Light rays, perpendicular to the light waves incident on the Hartmann plate, propagate from these holes creating spots on the CCD camera. When wavefront distortion is present, the positions of the spots change. Wavefront distortion, ΔW, can be calculated by dividing this displacement in centroid position, Δy, by the distance between the Hartmann plate and the CCD camera, L, and then numerically integrating the quotient.

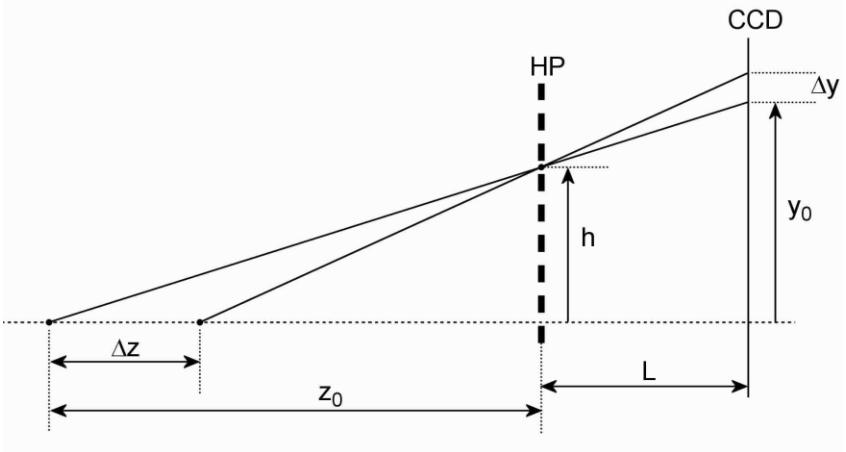

Figure 1: This diagram shows the change in spot positions, Δy, due to wavefront distortion along with the distance, L, between the Hartmann plate (HP) and the CCD camera, both of which are involved in calculating the wavefront change[3].

Thus, to calculate the wavefront distortion it is important to know the value of L and the change in centroid position to a high degree of accuracy. Centroid position is calculated accordingly,

$$\{x_c, y_c\} = \left\{ \frac{\sum_{ij} i I_{ij}^P}{\sum_{ij} I_{ij}^P}, \frac{\sum_{ij} j I_{ij}^P}{\sum_{ij} I_{ij}^P} \right\}\Bigg|_{P=2}, \qquad (1)$$

where I_{ij} refers to the number of photon counts in pixel (i,j). It has been noted that increasing the weighting reduces error, and in this case P = 2 was chosen for computational convenience[4].

Since the Adelaide group's development of an ultra-sensitive Hartmann sensor, they have looked for ways to reduce the sensor's thermal sensitivity. This has included replacing the brass Hartmann plate and aluminum clamp and spacer plates with plates made of invar. Invar is a steel alloy and has a very low coefficient of thermal expansion. They have also added heat sinks on each side of the camera to siphon off excess heat. The heat sinks are clearly visible on each side of the camera in the cover figure along with the invar clamp plate. Upon close examination the top side of the invar spacer plate can be seen behind the clamp plate and the invar Hartmann plate can be seen within the opening of the clamp plate.

The objectives of my project this summer were to find a way to raise the camera temperature by a few degrees and then test the modified Hartmann sensor's temperature sensitivity. I used MATLAB programs developed by Won Kim to both optimally set up the CCD camera and then, after taking pictures at different temperatures, to analyze the change in spot centroid positions.

Methodology

A. Calculating rms

The program centroid_statistics_raw_bygrid_opt_avg.m calculates and plots the rms values of the centroid positions at one temperature after averaging different numbers of frames.

The user specifies the number of frames that will make up the reference set and the number of frames that will make up the 'test' set that will be compared to the reference set. We usually took 5000 pictures, designated the first and last two thousand as the reference set, and designated the middle thousand (pictures 2001-3000) to be the test set. The program then stores rms values, calculated after averaging different numbers of frames, in a matrix. The set of numbers of frames are chosen by the user; for example for a set of 5000 pictures (or 1000 test frames), we usually specified the program to calculate and store in a matrix the rms values after averaging 1 frames, 2 frames, 5 frames, 10 frames, 20 frames, 50 frames, 100 frames, 200 frames, 500 frames, and finally 1000 frames. The program actually stores two matrices of rms values, one using a built-in MATLAB method of detecting the centroids, and another using an improved method of centroid detection that Won constructed.

The user also has to specify the file to obtain the pictures from and set three options at the beginning of the program to be true of false. These options are 'average_pixels', 'manual_bg', and 'shuffle_array'. Shuffle_array allows the user to shuffle the frames before calculating the rms, which, if the noise is purely random, should make no difference. Manual_bg allows the user to specify the background noise to subtract from the overall signal. Average_pixels is set true when using the brass Hartmann plate and aluminium clamp and spacer plates instead of the invar. When using these plates more significant diffraction occurs which causes the computer program to detect multiple centroid peaks within the same spot. Average_pixels blurs the spot images so that the computer still detects one centroid peak per spot.

Finally, the program also displays two plots of rms as a function of number of frames that have been averaged, one using the MATLAB rms values and another using the rms values calculated by Won's method. Each plot displays the theoretically predicted line of slope -0.5, the actual data, and the linear fit to that data. The program outputs the slopes of the linear fits, as well.

B. Analyzing Wavefront Change

Although using paraxial approximations can be very effective for a variety of calculations in geometrical optics, to determine the wavefront change to the degree of accuracy needed in Advanced LIGO it is necessary to take into account the aberrations implied by the higher order approximations particularly those contributed by the term $\frac{\theta^3}{3!}$.

$$\sin\theta = \theta - \frac{\theta^3}{3!} + \frac{\theta^5}{5!} - \ldots \qquad (2)$$

To describe the wavefront we have used the following equation:

$$W = P(x\cos\alpha + y\sin\alpha) + 0.5\,S\,(x^2 + y^2) + A\,(x^2 + y^2)^2 + 0.5\,C\,(x\sin\varphi - y\cos\varphi)^2 + B\,(x\cos\beta + y\sin\beta)(x^2 + y^2) \qquad (3)$$

The third and fifth terms describe the relevant third order aberrations, or Seidel aberrations, for the monochromatic light source being used. These are spherical aberration and coma, respectively. The first term is prism which describes the effect when wavefront is tilted off-axis with respect to a lens, the second term is spherical power which is proportional to the curvature

of the wavefront, and the fourth term is cylindrical power which describes how the wavefront curvature deviates from spherical form [3].

The program wf_aberration_temperature_bygrid.m performs a least squares fitting by calculating values for the wavefront aberration parameters from the transverse aberration of the spots in the x and y directions. It then uses these parameters to construct contour plots of the gradient of the wavefront change. It calculates the transverse aberration by detecting the spot centroids in two sets of spot images taken at different temperatures and calculating the displacement between the 'low temperature' spots and the corresponding 'high temperature' spots. As mentioned above,

$$TA_x = -L\left(\frac{\partial W}{\partial x}\right) \quad \text{and} \quad TA_y = -L\left(\frac{\partial W}{\partial y}\right) \qquad \text{(4) and (5)}$$

Using equation (3), one can evaluate equations 4 and 5 in the following manner:

$$TA_x = a_0 + a_1x + a_2y + 2a_3xy + 3a_4x^2 + a_4y^2 + a_5x^3 + a_5xy^2 \qquad (6)$$

$$TA_y = a_6 + a_2x + a_7y + 2a_4xy + a_3x^2 + 3a_3y^2 + a_5y^3 + a_5x^2y \qquad (7)$$

Let $\chi^2 = \sum_i$ $\{[TA_{xi} - (a_0 + a_1x + a_2y + 2a_3xy + 3a_4x^2 + a_4y^2 + a_5x^3 + a_5xy^2)_i]$

$+ [TA_y - (a_6 + a_2x + a_7y + 2a_4xy + a_3x^2 + 3a_3y^2 + a_5y^3 + a_5x^2y)_i]\}$ (8)

Assuming that χ^2 is a smooth, well-behaved function, the least-squares-method is used to determine the best estimates of the eight coefficients $a_0 \ldots a_7$. These coefficients are then used to calculate the values of the coefficients in equation 3. A contour plot of the gradient of the wavefront change can then be fitted to these parameters.

C. Camera Set-up

The two main frame grabber programs that helps interface the CCD with the computer are Pdv Show and Pdv Utilities. Pdv Utilities can be used to send commands to the camera. One of these commands that we frequently used measures the temperatures of the camera's digitizer board and sensor board. We also used a hand-held IR thermometer pointed at the heat sinks to take the temperature. These values were correlated with the computer measurements, indicating that the IR thermometer accurately measured relative temperature, if not absolute temperature.

Another command took a user-specified number of frames and saved them to a user-specified file. Pdv Show enabled us to take and visualize a still frame or the continuous frames that the camera was currently imaging. Pdv Show also included an option that displays the intensities of the current image being displayed, whether it was still or continuous. Pdv Show was very useful in ensuring the Hartmann plate was ideally aligned with the CCD and that none of the pixels reached saturation. In distinguishing different voltages detected by the CCD, the maximum intensity count is a function of the number of bits per pixel, n:

$$\text{Intensity count} = 2^n - 1 \qquad (9)$$

Thus, since we used a 12-bit camera, a pixel saturates when the intensity count reaches 4095.

In determining that the camera was set-up correctly we used the MATLAB code calibrationtest_opt_avg.m. After saving a still frame image using Pdv Show, the code would output the maximum pixel intensity of that image, the number of peaks detected in the image, a plot of the pixel intensity of each peak, and a plot that shows the locations of the centroids that were detected. This latter plot was useful in determining if some 'partial spots', spots that only partially fit onto the active surface of the CCD, were being detected. It was also important to ensure that pictures that were being compared had the same number of spots. Pictures were always taken with the lights of the room turned off.

Results

A. Results of Wavefront Aberration Analysis

My initial objective was to find a way to raise the temperature of the camera a few degrees Celsius so I could then proceed to comparing measurements of the spot positions at different temperatures. We started out by covering the top of each heat sink with a piece of lens cleaning tissue and then multiple pieces, hoping to heat the camera by interfering with the convection process that was cooling the camera. This method proved insufficient so we then tried covering the whole top of the camera and heat sinks with a single, and then multiple, pieces of regular white printer paper, cut to fit the shape. This also proved insufficient in raising the temperature even when the stack of paper was several sheets thick. We were finally able to successfully raise the temperature 2-3 degrees by creating a sort of "hat" for the camera and heat sinks. This "hat" consisted of several sheets of printer paper that covered not only the top of the camera and heat sinks but also draped the full length of the sides of the heat sinks, which proved sufficiently effective in disrupting the convection.

Once we found this way of increasing the camera temperature, we were able to start analyzing the centroid movement caused by temperature changes. We analyzed 5000 pictures taken at the camera's "room temperature"- its equilibrium temperature in absence of any heating devices- and 5000 pictures taken after this temperature was raised 4 degrees. After increasing the temperature we would expect the CCD plate to expand more than the Hartmann Plate (now made of invar with a very low coefficient of thermal expansion), causing the spots to appear as if they contracted, in a spherical pattern. The spherical pattern of centroid motion was observed by Aidan Brooks in the initial Hartmann Sensor, before it was modified to reduce its temperature sensitivity. However, after running the code to analyze wavefront change we calculated a larger value than expected for C, the coefficient in equation 3, indicating an unexpected, relatively large cylindrical component of the wavefront aberration. The value for C and the value for S, the spherical component, were both approximately on the same order of magnitude, 10^{-3}. Since this contradicted our expectations of the value of C to be much smaller than the value of S, we needed to determine whether this was a real signal, so we took measurements of the noise to make sure that the wavefront aberration noise was random.

We divided 2000 pictures, and later 5000 pictures, all at the same temperature into pairs of 200 pictures and compared centroid position changes for each pair. Using a MATLAB program, we calculated the S and C values for each pair, the overall average values for the spherical and cylindrical components, $\langle S \rangle$ and $\langle C \rangle$, respectively, and the standard deviation of the average values, σ_S and σ_C. If the noise was random, the average values should be

approximately zero. We expected <S> to be close to10^{-6} m^{-1}, but calculated a slightly larger value <S> = -8.28 * 10^{-6} m^{-1}, where $\sigma_S = 2.46*10^{-4}$. We calculated <C> = $7.03*10^{-5}$ m^{-1} and $\sigma_C = 2.65*10^{-4}$. So both averages were fairly small values as expected for random noise. Running the wavefront aberration analysis code we calculated the aberration parameters p, s, and c, for one of these pairs of 200 images all taken at the cooler temperature to be p = $9.77*10^{-7}$, s = $1.24*10^{-6}$ m^{-1} and c = $2.74*10^{-4}$ m^{-1}. We did the same calculation comparing frames all at the elevated temperature and found p = $3.35*10^{-7}$, s = $7.08*10^{-5}$ m^{-1}, and c = $-1.81*10^{-4}$ m^{-1}. However, for frames taken at different temperatures p = $4.50*10^{-5}$, s = $-2.5*10^{-3}$ m^{-1}, c = $1.22*10^{-3}$ m^{-1}. Thus for these samples prism and spherical power are both two orders of magnitude larger than their "noise values" and the cylindrical power is an order of magnitude larger than its "noise values".

We used MATLAB to construct contour plots of radial centroid displacement between cool images only, shown in Figure 2, and between hot and cold images, shown in Figure 3. The color bars roughly indicate the values of maximum and minimum spot displacements but are not correlated between plots.

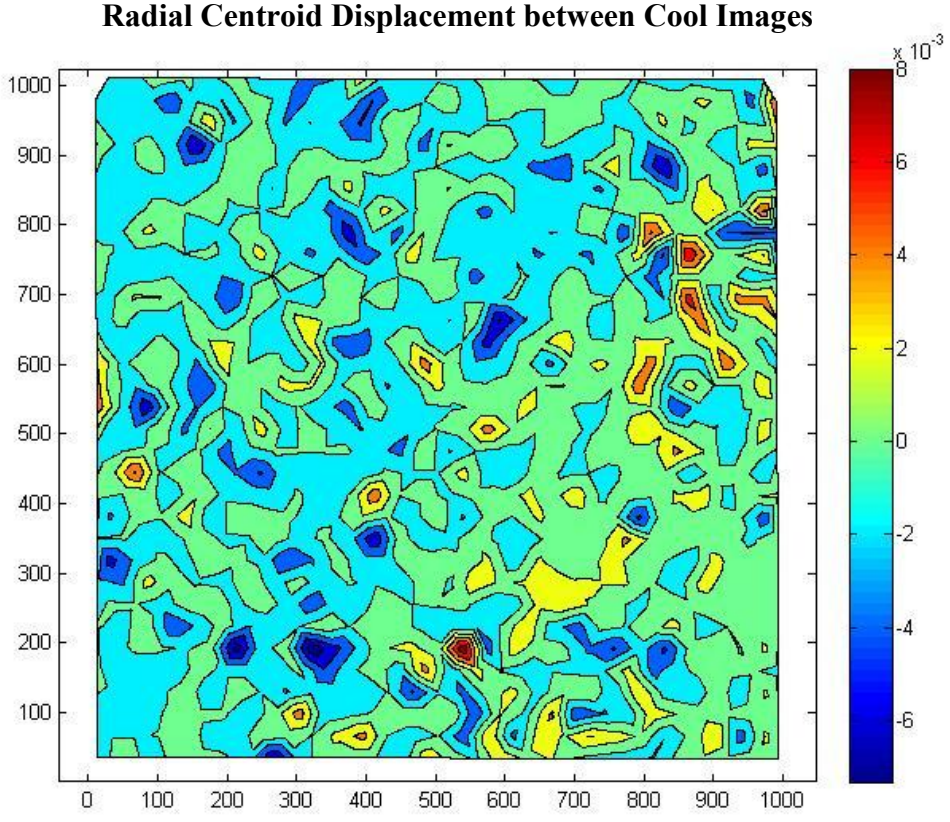

Figure 2: Contour plot of radial displacement between cool images only. The axes indicate pixel position.

Radial Centroid Displacement between Hot and Cool Images

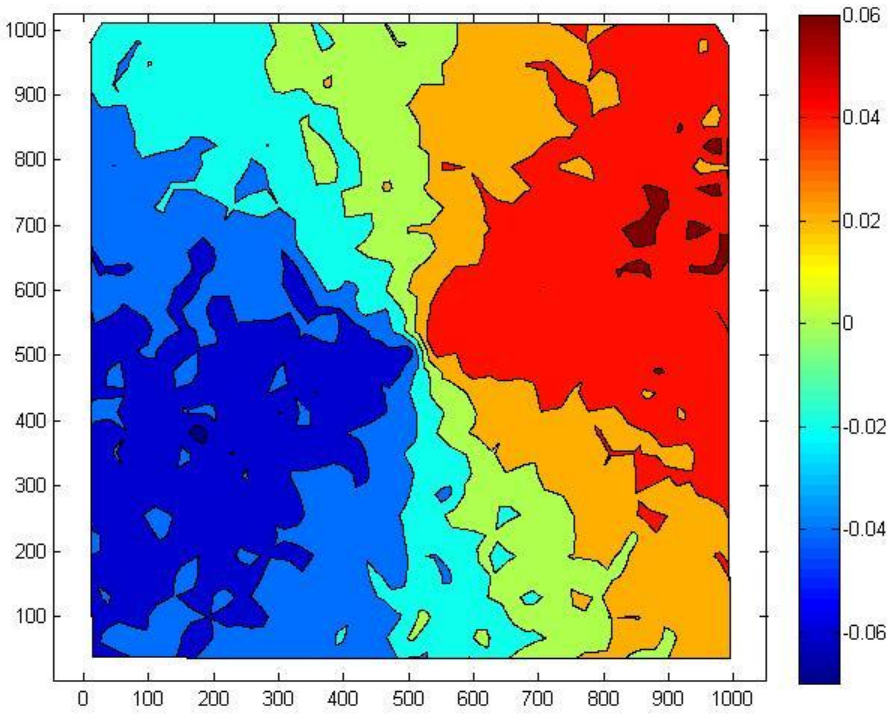

Figure 3: Contour plot of radial displacement between hot and cool images displaying cylindrical nature of signal. The axes indicate pixel position.

Figure 2 supports the conclusion that the noise is truly random since there is no obvious pattern or signal in the displacement and all values are relatively small. Figure 2 illustrates the cylindrical nature of the signal when comparing centroid positions at different temperatures with the magnitude of the signal being about an order of magnitude larger than the magnitude of the noise.

Since the cylindrical component of the signal seemed to be real, we started trying to discover its source since it was absent in measurements using the initial Hartmann sensor. To see if the cylindrical pattern was a feature of the heating method we decided to induce the temperature change by heating the room with the air conditioner, instead of using the "hat", and turning it off as soon as the sensor reached the desired temperature. We found that the temperature of the Hartmann Sensor did not change significantly during the measuring period after the air conditioning had been turned off. When analyzing the wavefront aberration using 5000 frames taken at room temperature and 5000 frames taken at a temperature elevated five degrees using this new heating method, we calculated $p = 1.49*10^{-4}$, $s = -1.42*10^{-3}$ m^{-1}, and $c = 5.86*10^{-4}$ m^{-1}. The cylindrical component was still clearly visible in the contour plot as well, indicating that this feature is independent of heating method.

Since there was a fairly strong prism in the signal as well, we decided to see if the cylindrical component was still present after removing the average prism. Again we took 5000 pictures at room temperature, 200 pictures at a temperature elevated about one degree, and 5000 more pictures at a temperature elevated about five degrees. Figures 4 and 5 display the contour plots of centroid displacement before removing prism for the one degree increase in temperature

and the five degree increase in temperature, respectively. Before removing prism the aberration parameters when comparing the frames with a one degree temperature difference were calculated to be $p = 1.46*10^{-5}$, $s = 1.78*10^{-4}\ m^{-1}$, and $c = -1.47*10^{-4}\ m^{-1}$. For the five degree temperature difference they were calculated to be $p = 1.46*10^{-4}$, $s = -1.58*10^{-3}\ m^{-1}$,and $c = 1.31*10^{-3}\ m^{-1}$. Figures 6 and 7 display the contour plots of centroid displacement after removing prism. Once again the color bars are not completely correlated between images.

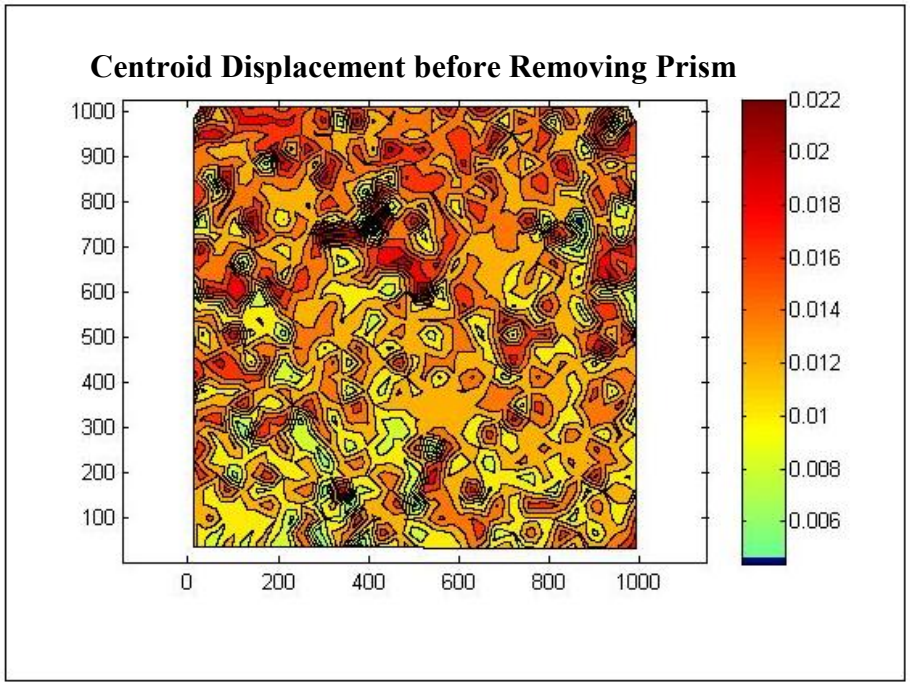

Figure 4: Contour plot of centroid displacement between images taken at temperatures 1 degree apart. Axes indicate pixel position.

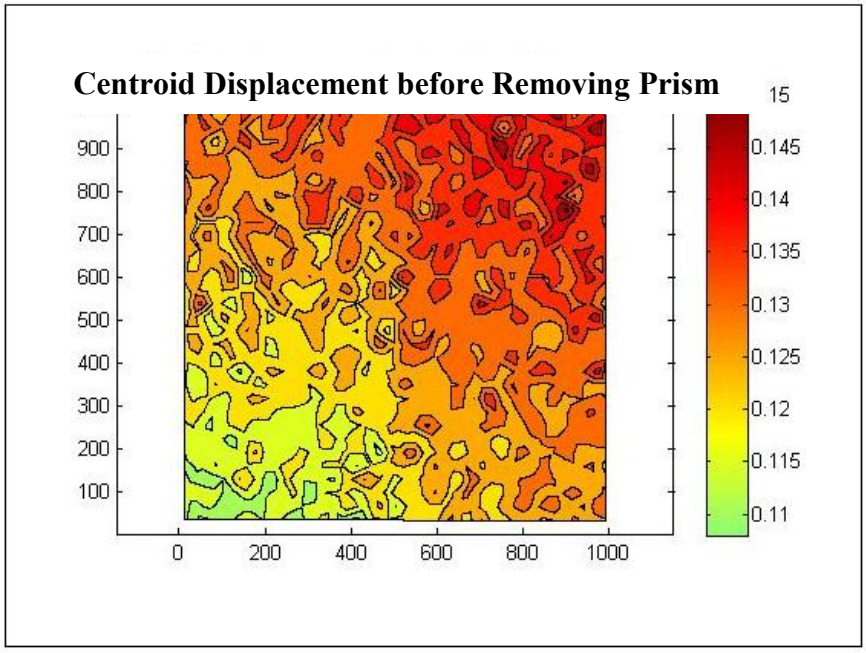

Figure 5: Contour plot of centroid displacement between images taken at temperatures 5 degrees apart. Axes indicate pixel position.

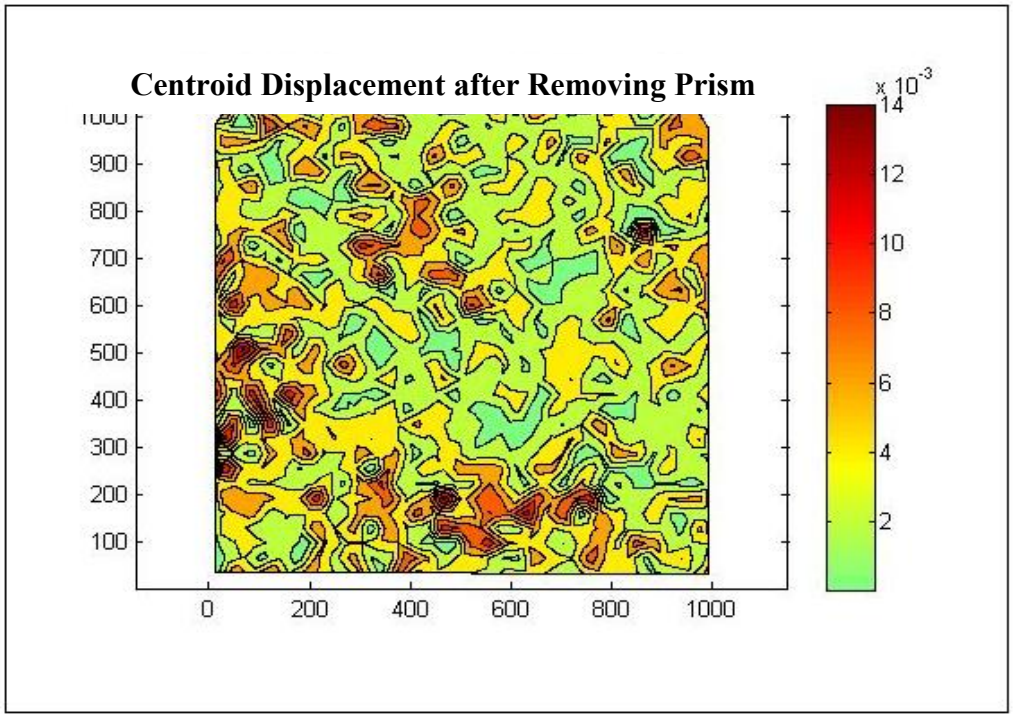

Figure 6: Contour plot of centroid displacement between images taken at temperatures 1 degree apart. Axes indicate pixel positions.

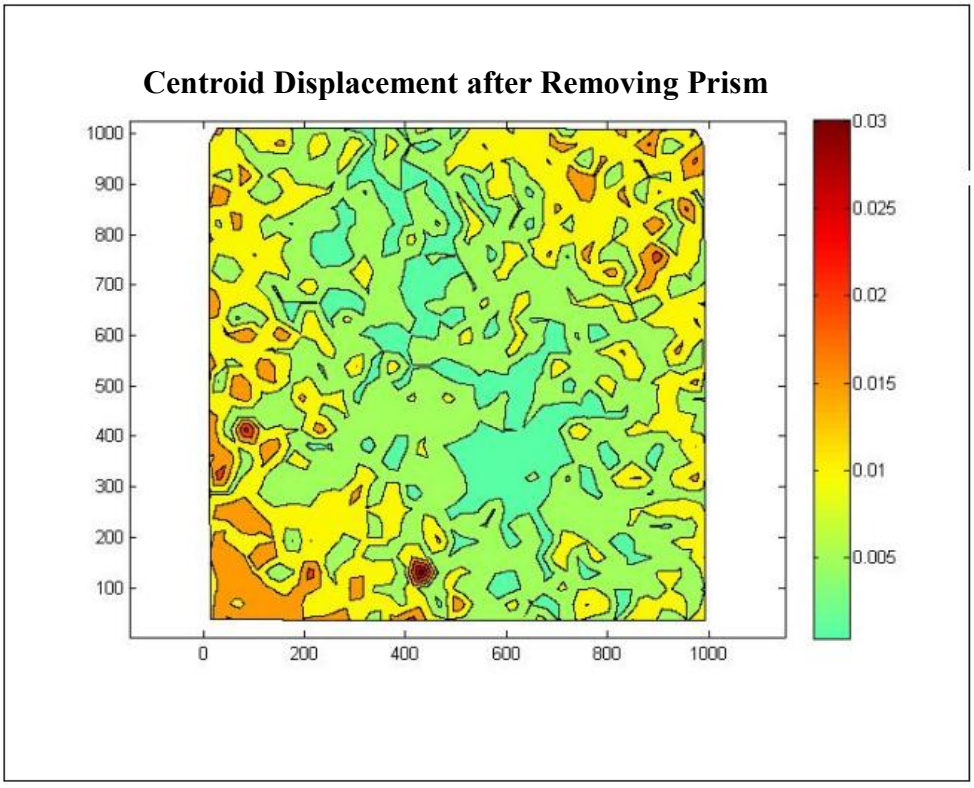

Figure 7: Contour plot of centroid displacement between images taken at temperatures 5 degrees apart. Axes indicate pixel position.

The displacement in the plots comparing frames taken at room temperature and frames taken after increasing the temperature by one degree appears more random. As the room temperature frames are compared with frames taken at higher temperatures, the displacement plots become more organized. We later took similar measurements incrementing the temperature by one degree for ten degrees. The subsequent contour plots of the displacement also were more random when comparing frames at temperatures a few degrees above the initial equilibrium temperature and became more organized into a cylindrical structure as the temperature of the test frames increased. Although not as obvious as in Figure 5, there still seems to be a strong cylindrical component in Figure 7, indicating that removing the prism did not remove the cylindrical power.

Deciding the cylindrical power might arise from some effect within the Hartmann sensor we then took measurements after doing a series of different tests to try to determine the source. After each test I made a plot of the wavefront aberration by constructing a best fit to the previously calculated wavefront aberration parameters. Won also designed code to numerically integrate the gradient of the wavefront aberration. Figures 8 and 9 are typical samples from our following tests. In all our plots and calculated parameters the cylindrical feature was present and with approximately the same magnitude. The aberration parameters for the following two figures were as follows:

P: $1.89*10^{-4}$
al: -0.295
phi: 0.196
C: -0.00159 m^{-1}
S: -0.00383 m^{-1}
B: 0.0983 m^{-2}
be: -0.376
A: 5.97 m^{-3}

where al, phi, and be represent the angles α, φ, and β in equation 3 (P, S, C, A, and B are the other coefficients from that equation).

First we rotated the Hartmann plate along with the clamp plate 90 degrees and the axis of the cylindrical pattern rotated 90 degrees. The Hartmann plate had been attached to the clamp plate using tape on two of the four sides, so we cleaned the Hartmann plate, removing all tape and leftover glue, to make sure that the tape was not applying any unusual stresses under the temperature change that could be causing the cylindrical effect. However, measurements with the clean Hartmann plate still showed the cylindrical effect. We then rotated just the Hartmann plate 90 degrees and the axis of the cylindrical pattern rotated but only by a small amount, roughly 15 degrees. Measurements taken after returning the Hartmann plate to its original position showed that the axis of the cylindrical pattern also rotated back in the direction of its original position, though not completely. Rotating just the invar plate by 90 degrees also did not seem to have an obvious effect on the cylindrical pattern which rotated but only by a small amount, similar to the result when just rotating the Hartmann plate.

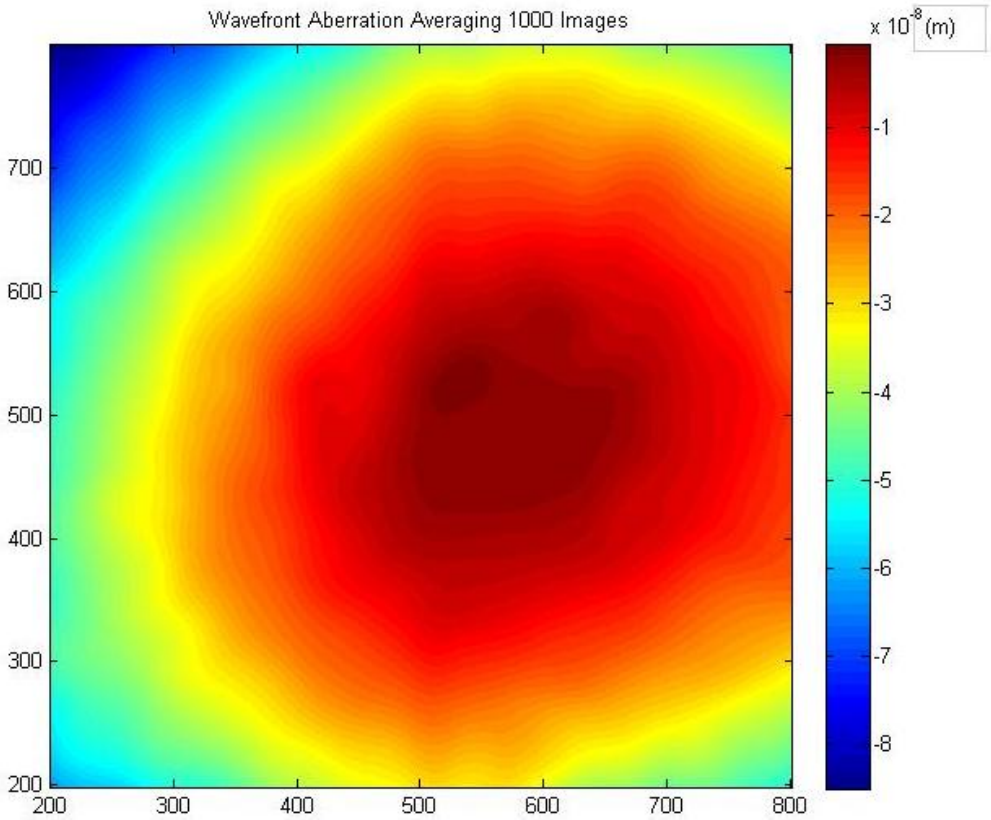

Figure 8: This is a contour plot of the actual wavefront aberration comparing room temperature frames with frames at a temperature 10 degrees higher. This plot was obtained by numerically integrating the gradient of the wavefront aberration. Note the cylindrical nature of the signal.

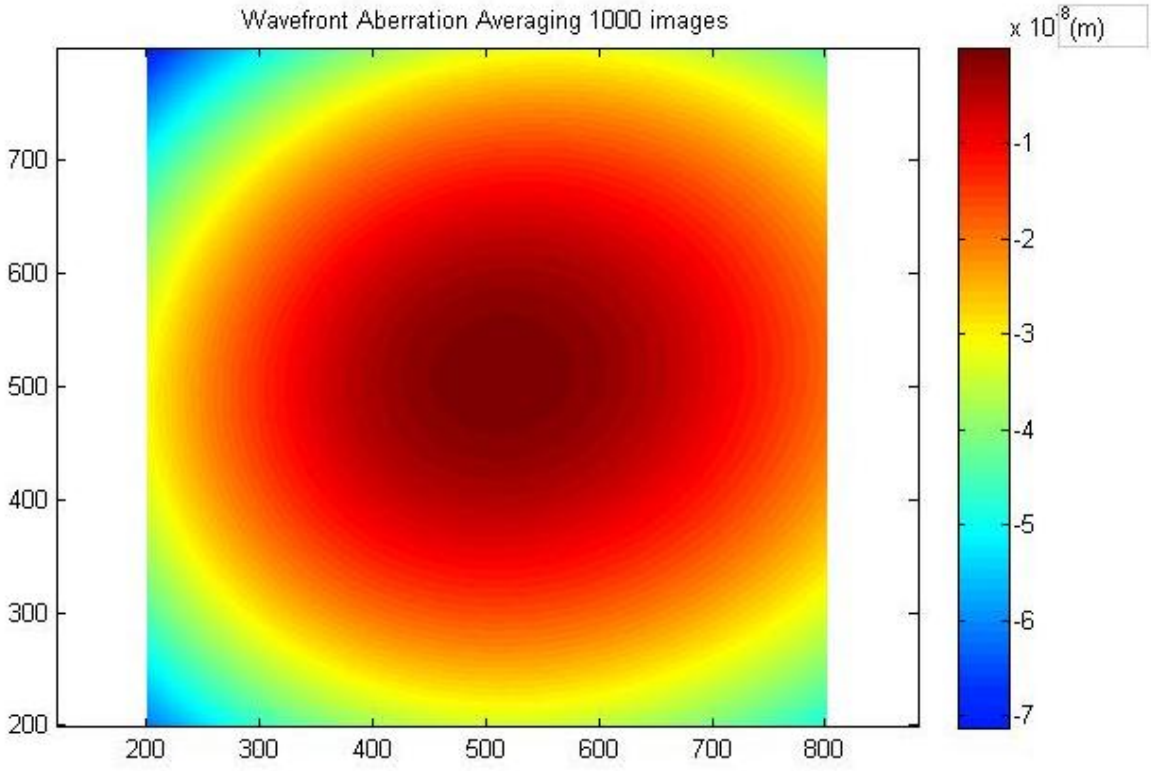

Figure 9: This contour plot is a best fit of the wavefront aberration using the wavefront aberration parameters. So consequently it has a smoother appearance. The cylindrical shape is also clearly noticeable in this plot.

B. RMS Analysis

While continuing to run these tests we decided to switch our focus to another problem with the rms calculations that had been present simultaneously. As mentioned above, when plotting rms as a function of number of frames averaged, rms was theoretically predicted to drop with a slope of -0.5. When using our MATLAB routine to calculate the rms, we calculated it twice, with and without shuffling the frames before the calculation. When the frames were shuffled prior to calculating the rms, the slope would closely match the theoretical prediction, however when the frames were not shuffled, the calculated slope would be significantly lower. The fact shuffling improved the rms implied that the noise was not purely random and that the centroid positions in each frame were not statistically independent events. Since this discrepancy between rms values before and after shuffling was present in all previous measurements, we decided to not analyze the wavefront aberration until we found the source of the rms problem first. It is also possible that the solutions to both problems could be related.

Figures 10 and 11 show typical rms plots both with and without shuffling the frames. The following are the corresponding rms values after averaging 1, 2, 5, 10, 20, 50, 100, 200, 500 and 1000 test frames with and without shuffling. 4000 frames were used as reference frames making 5000 frames total. Without shuffling:

Frames Averaged	rms
1	0.004961805627314
2	0.004537271715921
5	0.004208328351279
10	0.004042641862253
20	0.003490778156514
50	0.002924351382593
100	0.002130578225855
200	0.001944384005894
500	0.001687318461522
1000	0.000881173809942

With shuffling:

Frames Averaged	rms
1	0.004018866673087
2	0.002724680286563
5	0.002319477846009
10	0.001230553835673
20	0.000767638027270
50	0.000432681002432
100	0.000427139665006
200	0.000270955332752
500	0.000226521040455
1000	0.000153760240692

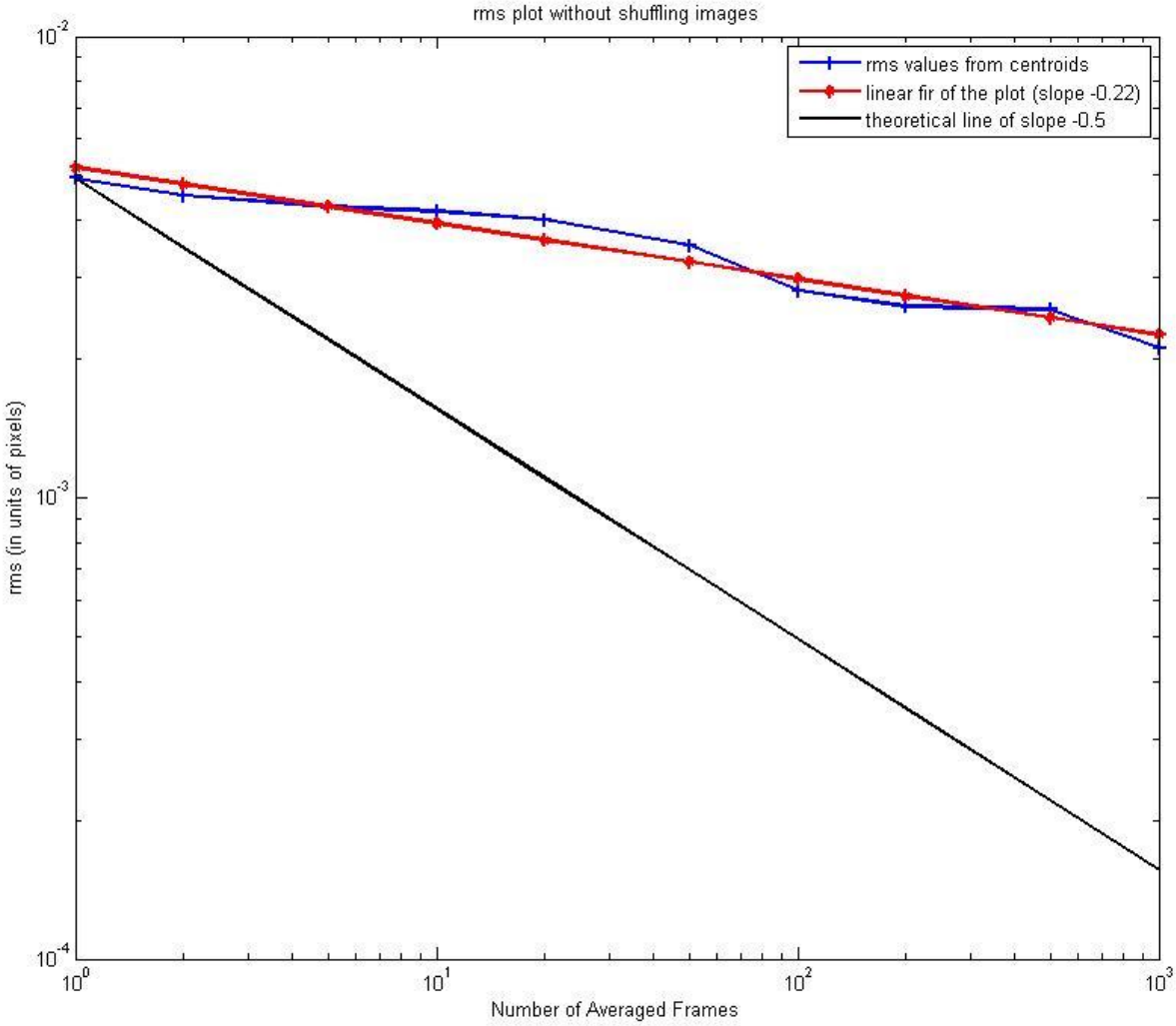

Figure 10: rms plot without shuffling. The slope of the linear fit is included in the legend.

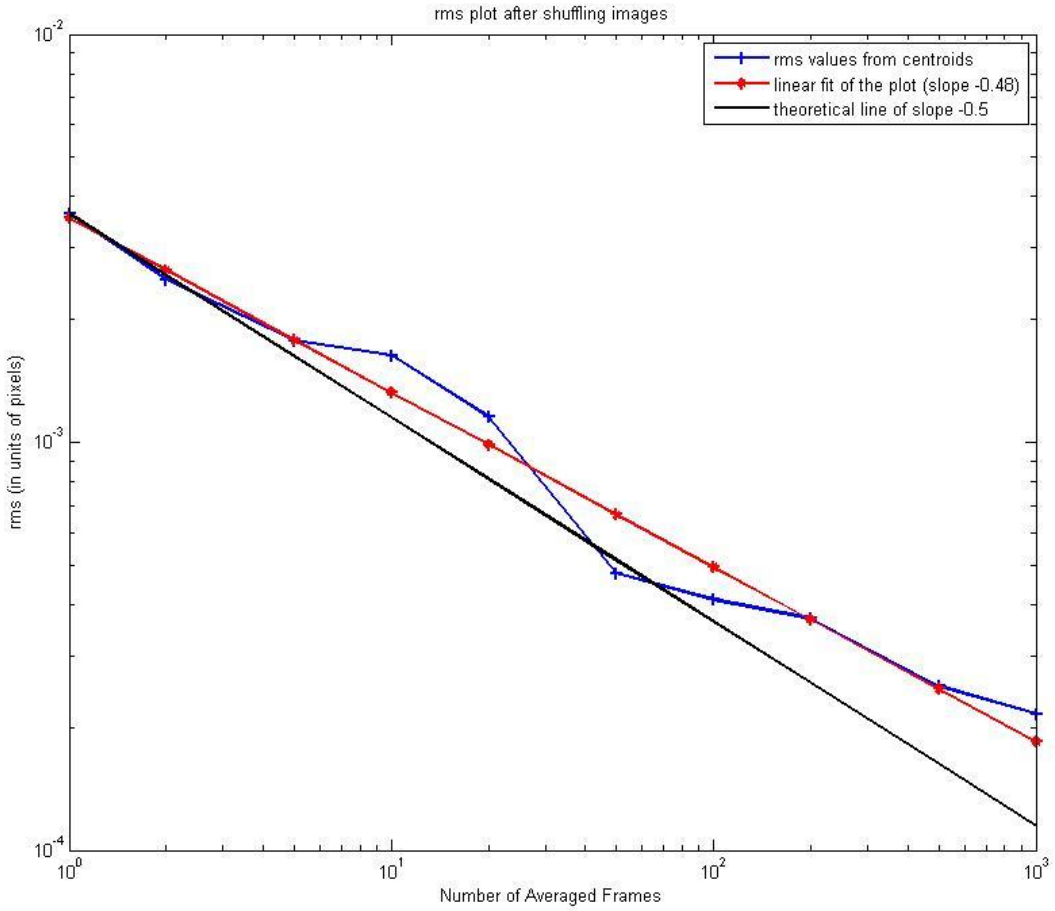

Figure 11: rms plot with shuffling. The slope of the linear fit is included in the legend.

At this point we decided to take measurements using a brass Hartmann plate and thicker aluminum clamp and spacer plates, like in the initial Hartmann sensor, since this cylindrical component was not detected when using that sensor. Also, since the invar plates are thinner than the aluminum plates, they would be more susceptible to having been bent or damaged while being manufactured which might also cause the cylindrical effect. Greater diffraction was present when using the brass and aluminum set up of the Hartmann sensor causing the centroiding routine to detect multiple centroids per spot. Won fixed this by creating a MATLAB routine that would blur the spots thus causing the program to correctly recognize spots and their centroids. This function can be toggled on and off in the rms and wavefront aberration programs by setting "average_pixels" to be true or false. However, this did not alter our unusual rms results so we concluded that the source of the problem may be related to the way we take the pictures or the environment the sensor is in.

To test this we replaced the CCD with a new, unopened and unused camera and took more pictures. The analysis of these pictures showed that replacing the camera made no difference. We then decided to take pictures using the new camera but with the invar Hartmann, clamp, and spacer plates of the modified Hartmann sensor instead of the brass and aluminum

plates. This was to verify that Won's coding to smooth out the pixels was not contributing to the problem. Since this also did not affect our rms results, this validated Won's coding. Won also created code that made a contour plot of the log of the rms. This plot made "bad spots", spots where the rms was particularly high, more easily visible. We made contour plots of different sets of data, as well as contour plots comparing different subsets of frames within the same set of data to see if the "bad spots" were always the same spots. Figures 12, 13 and 14 are plots comparing different subsets of "bad spots" and demonstrate that the "bad spots" were not reproducible. Similarly we looked at these types of plots to see if at least there were other patterns, such as whether or not the number of bad spots increased with time (with later frames), but there did not seem to be any obvious patterns.

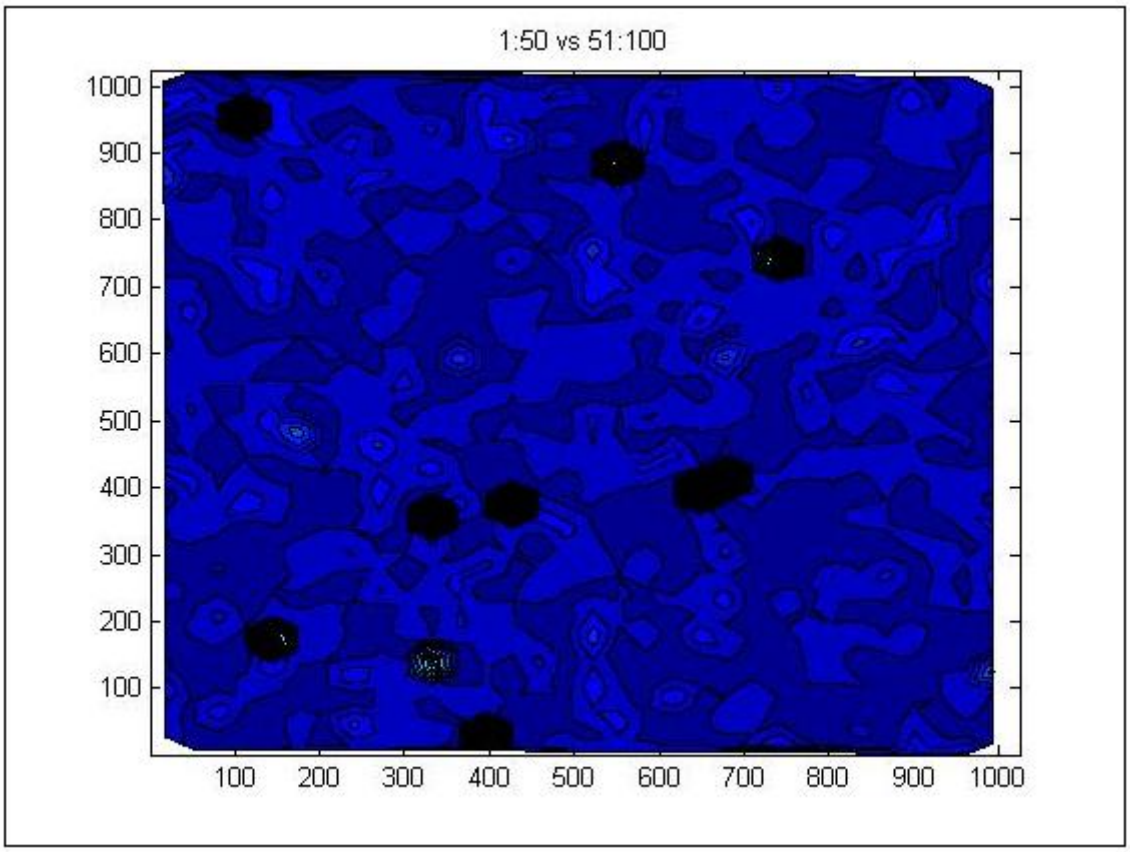

Figure 12: This plot shows the "bad spots" when comparing the first 50 frames, the reference set, to the next 50 frames. Axes indicate pixel position.

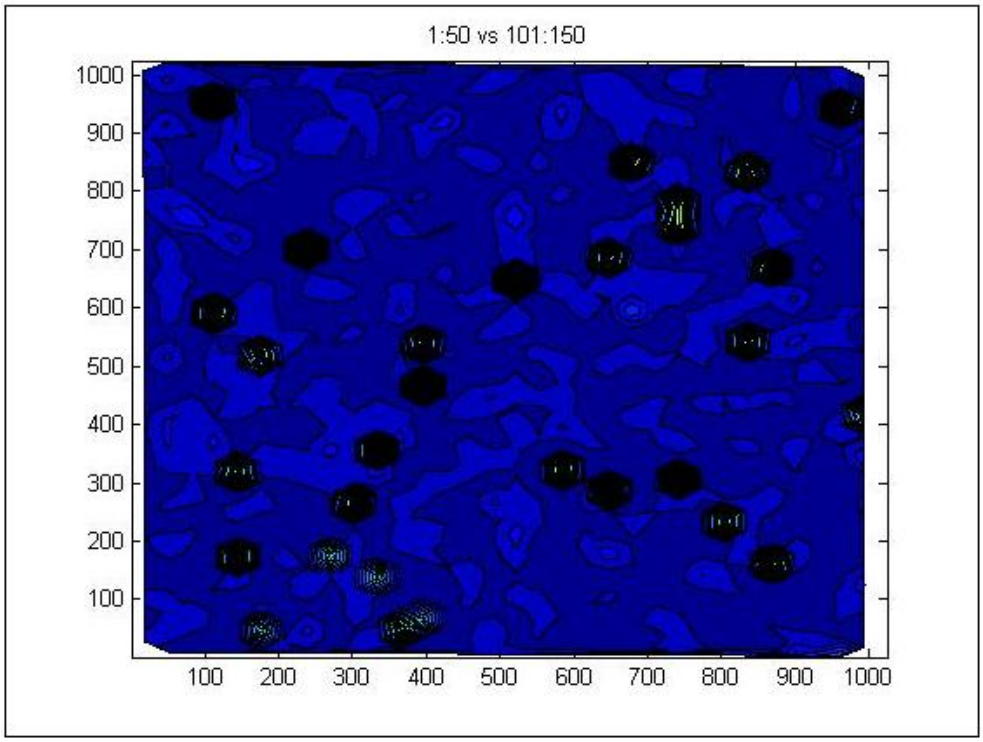

Figure 13: This plot compares the same reference set to the following set of 50 frames. Some bad spots shown in Figure 12 seem to carry over, but not all. Also, significantly more bad spots appear in this figure. Axes indicate pixel position.

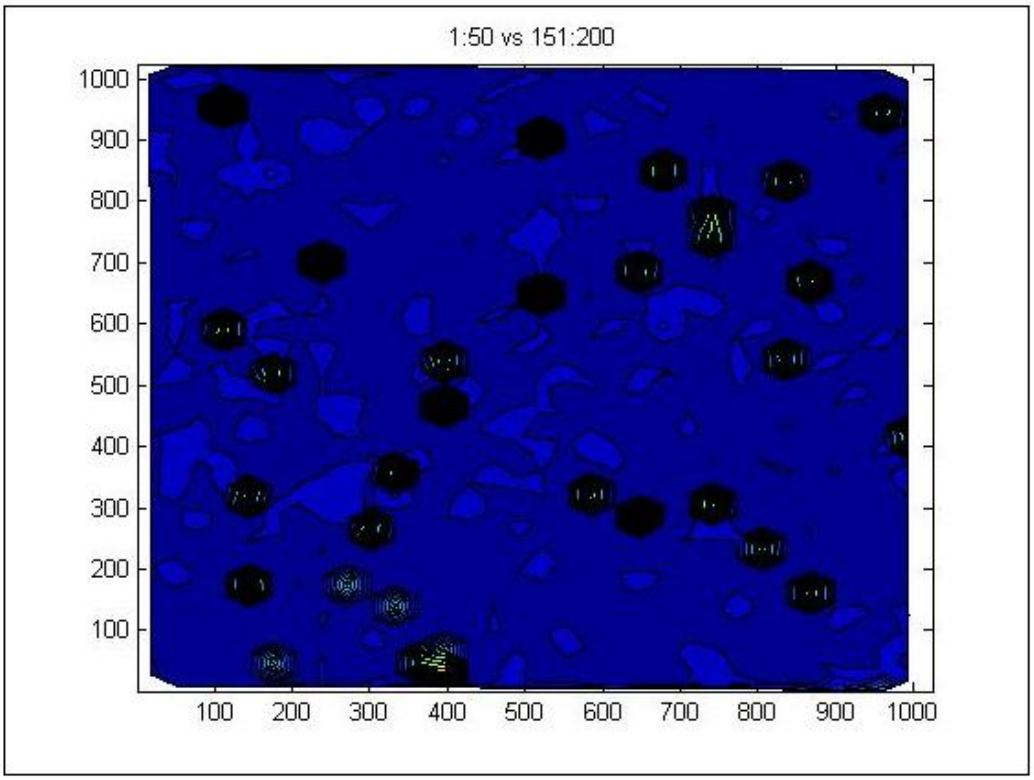

Figure 14: This plot compares the same reference set to the following set of 50 frames. Axes indicate pixel position.

We also decided to try manually subtracting the background noise instead of using the built-in MATLAB method. To subtract this background noise we took pictures while completely covering the camera's aperture and then subtracted the average of this signal manually. This is the same signal being subtracted if "Manual_bg" in the rms code, mentioned above, is set to be true. However, more measurements revealed that this did not seem to affect the rms results. We also modified the way the average prism was removed from each frame by using the following routine:

(1) Centroid all spots
(2) Calculate the average of all centroids in frame *i*, $(\bar{x}_i, \bar{y}_i)$
(3) Subtract $[(\bar{x}_i, \bar{y}_i) - (\bar{x}_1, \bar{y}_1)]$ from all centroids in *i*th frame, $i \neq 1$.
(4) Average centroids for each spot over N frames, where N is the total number of frames

This more precise and time consuming code, however, did not seem to impact the rms results either. We also checked if this method of removing prism affected the wavefront aberration results, but it did not.

Since the Hartmann sensor was in an open set-up on a lab table whereas the initial Hartmann sensor was tested inside a tent that protected it against air currents, we decided to test how sensitive the Hartmann sensor was to air currents. I took 5000 frames, which takes about 3.5 minutes, and gently waved a piece of paper next to one of the heat sinks of the camera for the last minute of measurement. Using Won's coding we constructed plots of the centroid drift for specific spots and plots for the average centroid drift, shown in Figures 15-18. The effect of the induced air disturbance in these plots is obvious.

Since the simple air disturbance had such a great affect on centroid position and I had been fanning by one of the heat sinks we decided to take measurements without the heat sinks. This would help determine whether the acoustic noise from the air currents themselves or the disruption they caused in the convective cooling process had the greater effect on centroid displacement. The rms was still high before shuffling though, indicating that this effect was independent of the heat sinks.

Frames Averaged	rms
1	0.003722961917501
2	0.003722961917501
5	0.003044823304032
10	0.002884934135984
20	0.002748699189918
50	0.002538889952250
100	0.002270514510127
200	0.002152777803032
500	0.002401487295145
1000	0.001062481663045

The slope of the linear fit was approximately -0.13, much lower than the theoretically predicted value of -0.5.

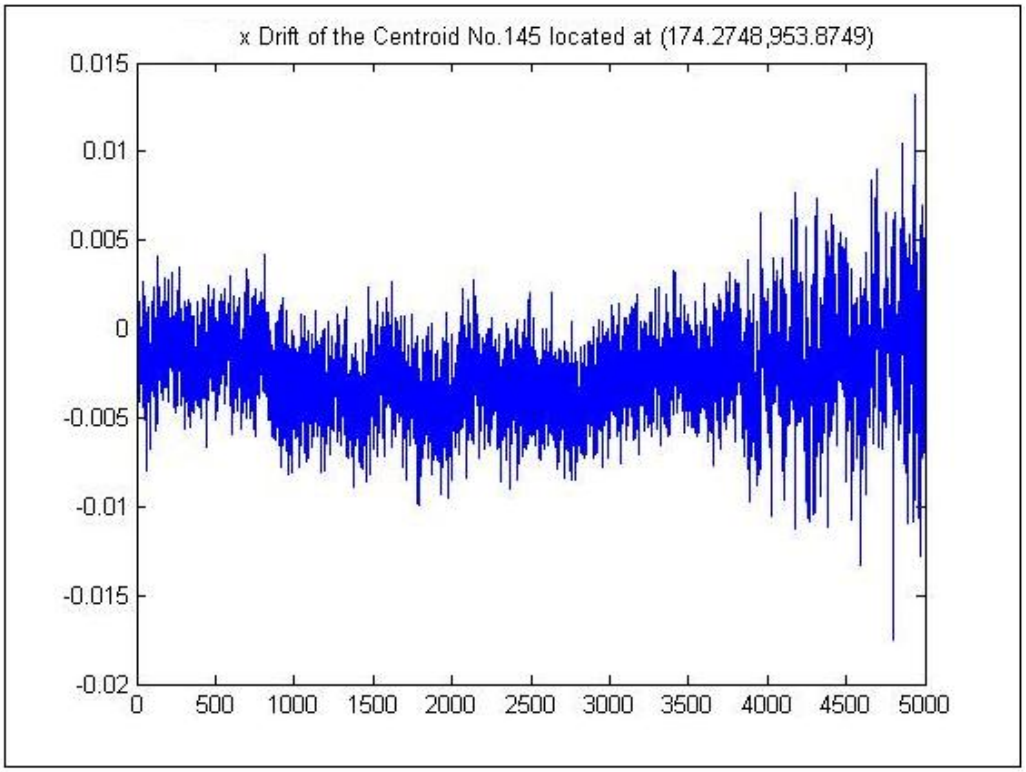

Figure 15: x drift of the centroid of spot 145. The numbers in parenthesis is the location of the centroid in pixels. The y axis represents displacement in units of pixels, and the x axis represents frame number. The effect of the fanning can be clearly seen in increase in rms for the last 1000 frames.

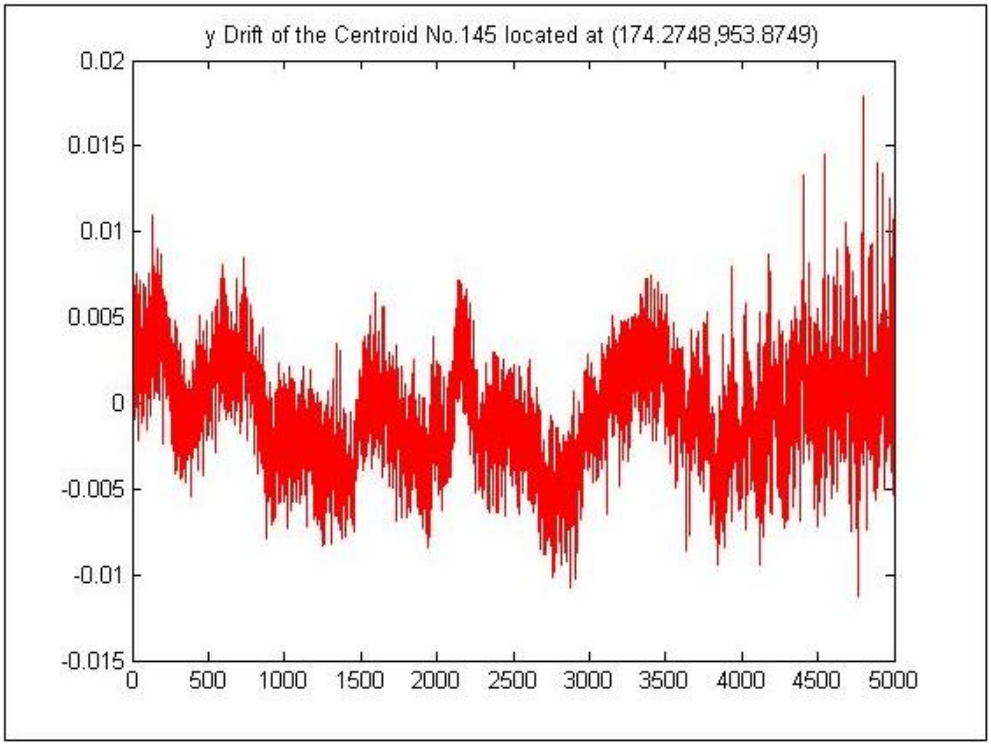

Figure 16: y drift of the centroid of spot 145. The y axis represents displacement in units of pixels, and the x axis represents frame number. Once again, the effect of the fanning can be clearly seen in increase in rms for the last 1000 frames.

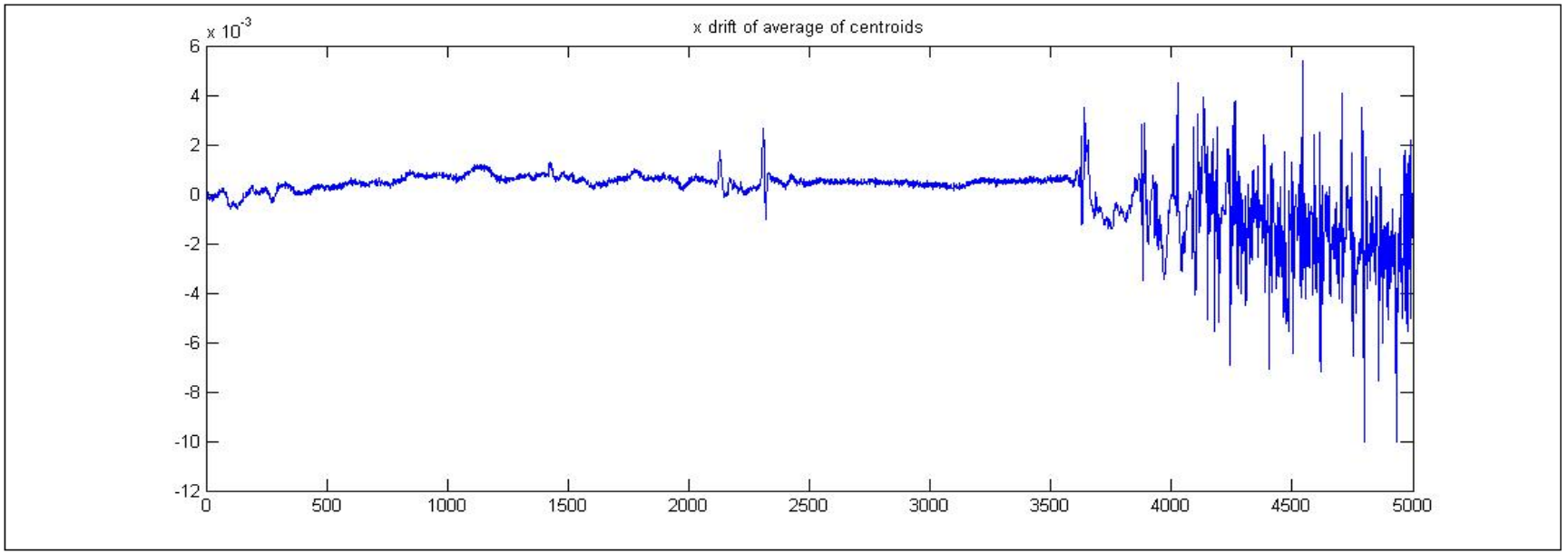

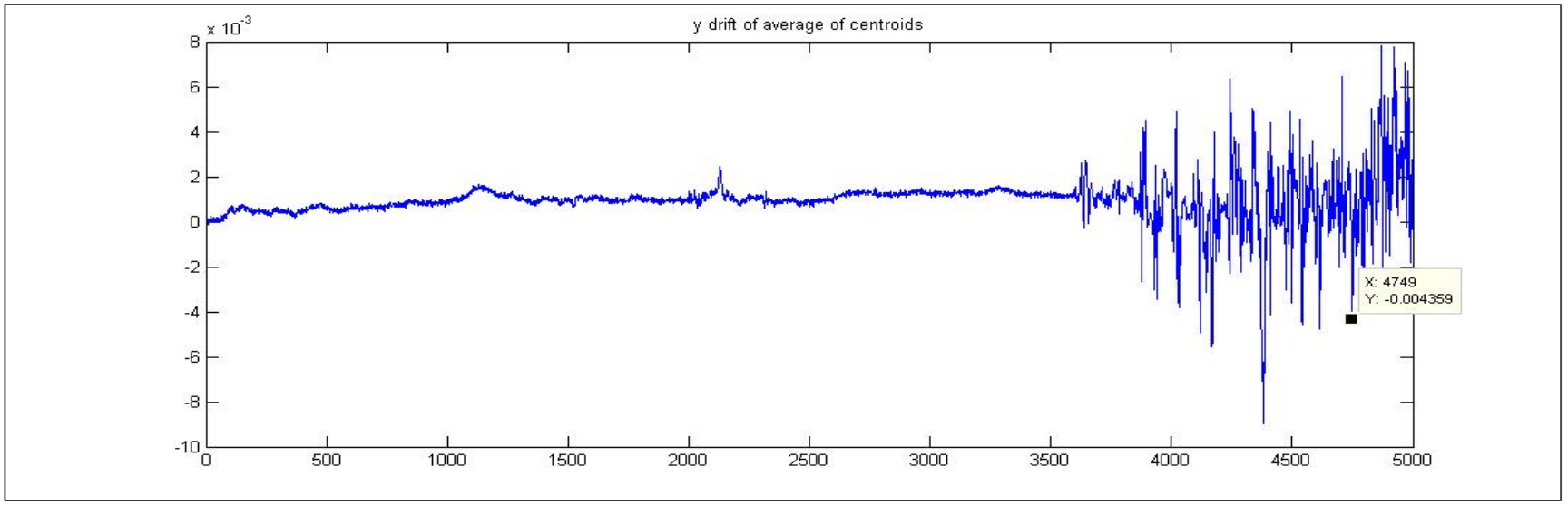

Figures 17 and 18: Average centroid drifts in x and y directions. y axis is displacement in units of pixels and x axis is frame number. The disturbance caused by the air fanning is most obvious in these plots.

Conclusion

Although we did not find the source of the cylindrical power or the cause of the discrepancy in rms values calculated with and without shuffling beforehand, we did successfully conduct tests on the Hartmann sensor on a more in-depth scale than had been done previously and narrow down the variables that could factor into these problems. We found that the cylindrical component was not a feature of heating method and that removing the average prism value did not affect the cylindrical component. We also found that although the axis of the cylindrical component rotated 90 degrees when we rotated the Hartmann plate and clamp plate together 90 degrees, it rotated a very small amount when we rotated just one of those plates 90 degrees.

For the rms analysis we found that all the factors just mentioned did not affect the need to shuffle the frames in order to achieve an rms close to the theoretical prediction. We also found that switching back to the brass and aluminum set-up of the Hartmann sensor, switching CCD cameras, modifying the code for removing average prism, subtracting the MATLAB created background noise, and removing the heat sinks did not affect the rms. We did discover however that there were irregular spots where the rms was particularly bad although we could not identify a pattern in their occurrence. Similarly the centroid displacement of certain spots and the average centroid displacement were much larger than expected, and that slight air disturbances could have a significant effect on centroid displacement.

Future experiments should include calculating rms after taking data with a tent enclosing the Hartmann sensor to prevent air currents from interfering with measurements. Moving the Hartmann sensor to a different lab table and room to see if the rms problem is a feature of the environment, such as electrical noise from the outlets, should also be done. Also acquiring a new frame grabber could test if the current frame grabber is the source of the problems.

Acknowledgements

I would like to thank the National Science Foundation (NSF) for funding my research, the University of Florida Physics Department for organizing and offering me this opportunity, and the University of Adelaide Optics Group for hosting me. Specifically I'd like to thank Peter Veitch for advising me and Won Kim who developed the MATLAB programs and worked very closely with me in conducting the various experiments.

References

[1] http://www.ligo.caltech.edu/advLIGO/scripts/summary.shtml

[2] Brooks, Aidan, et al. Direct measurement of absorption-induced wavefront distortion in high optical power systems. Applied Optics. 48, 355-364 (2009).

[3] Brooks, Aidan, et al Ultra-sensitive wavefront measurement using a Hartmann sensor. Optics Express. 15. 10370-10375 (2007).

[4] Brooks, Aidan, et al. Direct measurement of absorption-induced wavefront distortion in high optical power systems. Applied Optics. 48, 355-364 (2009).